Journal of Research and Applications in Mechanical Engineering
ISSN: 2229-2152 (Print); 2697-424x (Online)
(2023) Vol. 11, No. 2, Paper No. JRAME-23-11-010
[DOI: 10.14456/jrame.2023.10]

Research Article

Design and Analysis of a Novel Vertical Axis Water Turbine for Power Generation from Water Pipelines Using K-Epsilon and SST K-Omega Model

W. Lahamornchaiyakul
N. Kasayapanand*
Division of Energy Technology, School of Energy, Environment and Materials, King Mongkut's University of Technology Thonburi, Bangkok 10140, Thailand

Received 24 November 2022
Revised 15 March 2023
Accepted 8 May 2023

Abstract:
The research presents the proposed results of the design and analysis of the performance of a novel vertical axis small water turbine for power generation from water pipelines using the computational fluid dynamics (CFD) technique by using the turbulence model applications of the K-epsilon and SST K-omega. The turbines have a diameter of 40 millimeters, and the simulated water wheel consists of a set of two wheels. According to the study, numerical simulation effects in combination with K-epsilon and SST K-omega turbulence models could predict the mechanical power of pipeline water turbines conforming to theoretical principles. The results showed that the opening deflector domain at a water flow rate of 0.02 m^3/s was able to produce a maximum rotation speed of 435.67 rpm, a maximum torque of 0.74 N.m, and could generate maximum mechanical energy when calculating the rate of energy loss from the pipe system equal to 10.2 watts.

Keywords: *Water turbine for installation in pipeline, Turbulent flow simulations, Computational fluid dynamics, Numerical simulation*

1. Introduction

Saving water and energy has been one of the biggest issues in the globe over time, and it is predicted that this trend will continue in the near future [1]. Hydropower is generated by water flow, which can be considered a clean source of energy and does not affect the environment. The concept of developing energy patterns generated by water flow has played an important role over the years in countries, as groups of these countries have begun to fully understand the importance of environmental sustainability [2]. At present, Thailand has been researching more and more forms of energy generated by fluid flow, especially wind and hydropower. Both forms of energy can extract electrical energy through torque which can be produced from flow currents. However, both forms have limitations in their use. For example, there is a downside to the uncertainty of various seasonal wind streams. Hydropower is more stable because it is more uniform since the flow of water has a higher flow energy density [3]. The current design and development of small power generation turbines are very common in Thailand. Water turbines can be divided into two main types: horizontal-axis water turbine generators (HAWTG) and vertical-axis water turbine generators (VAWTG). When considering both power generation and water turbines, it is found that horizontal-axis power turbines can generate more energy with higher efficiency than vertical-axis water turbines, but a vertical-axis water turbine also has the advantage of reducing installation space [3, 4].

* Corresponding author: N. Kasayapanand
E-mail address: nat.kas@kmutt.ac.th

As a result of the operation of the vertical power generation water turbine, the advantages of the vertical-axis water turbine are applied to the flow system in the pipeline with many waters delivery lines in each country of the Irrigation Department. Researchers and engineers have studied and designed the vertical water turbines used in the pipeline system. Based on that principle, it can be considered one of the new policies aimed at taking advantage of the flow rate of water distributed along the water supply network [5], and beyond that, solving the problem of piping systems causing excessive pressure. This gave rise to a new concept and proposed modification of pressure-reducing valves for energy production equipment [5, 6] to systematically and efficiently enumerate energy production and ensure maximum efficiency and properly control the water pressure in the water supply pipeline system [7]. According to measures to investigate the installation of water turbines in water pipeline systems, there are many stages of the extraction process that may be transformed into electrical energy via flow patterns inside the pipeline. It enables the use of sustainable energy sources, which are sometimes overlooked in bodies of water, to minimize reliance on local energy, networks, and system running expenses [5, 8]. According to previous research papers, many different types of core water turbines are installed in piping systems, either as spherical [8] or with other types of water turbine blade shapes that resemble spherical patterns, as presented in Fig. 1.

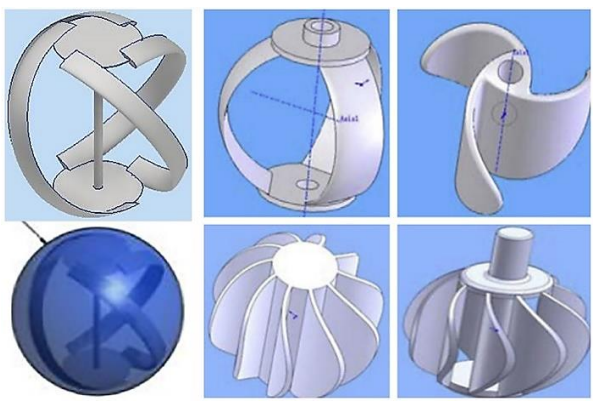

Fig. 1. Illustrates small turbines used in water pipeline systems based on research publications [1, 5, 8].

The design was developed with CFD simulation (computational fluid dynamics analysis). The simulation process starts by presenting the behaviour and flow patterns of water flowing through the developed spherical water turbine wheel with a package from the ANSYS CFX program [9]. The design and analysis of the rotation of most power generation turbines are formed as a turbulent flow. Thus, the simulation of fluid dynamics results. What indicates the accuracy of the numerical results is turbulence models such as the standard k-epsilon turbulence model and the SST k-omega turbulence model based on research over the years. The standard k-epsilon turbulence model is very commonly used because it saves calculation time and is accurate for a wide range of turbulent currents [10, 11]. The SST k-omega turbulence model is suitable for use to perform flow pattern analysis in viscous subclasses. In other words, it is possible to simulate both flows under isolation and flow under an adverse pressure gradient well [12].

In this study, the researchers proposed using both turbulence models to simulate the rotation of two axially small turbines used for installation in a water pipeline system, as shown in Fig. 2 and then comparing torque, mechanical power, and various flow fields such as pressure flow field, velocity flow field, blade edge velocity, and so on.

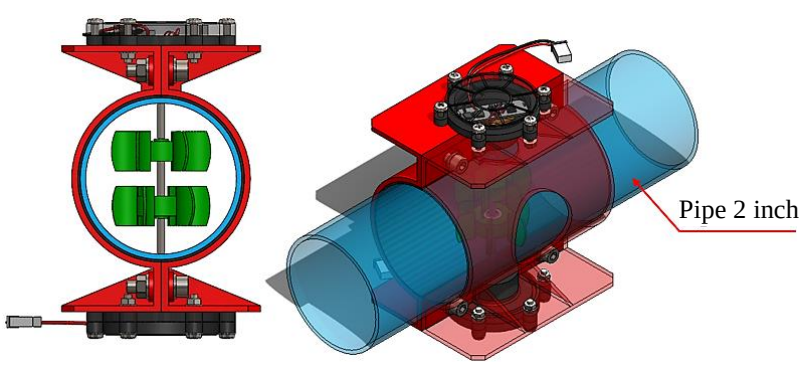

Fig. 2. A novel vertical-axis small water turbine model for the case study.

2. Material and Methods

2.1 The Software for the Calculation of the Results

In this research, the researchers used the Autodesk Flow Simulation program to help calculate the rotation cycles. Torque calculation using Autodesk Flow Simulation can fully support the use and analysis of variables, with the choice of a variety of turbulence models. Moreover, it is easy to prepare models for the analysis of the material properties. Determination of rotational element mesh includes configuring the rotation to calculate torque, mechanical power, etc.

2.2 The Design Data

In this research, the researchers adopted a new vertical axis water turbine model for the generation of electricity from two of the water turbines wheels, which had been redesigned, and proposed design approaches for both the left and right frames that serve to bind to the structure of the water pipe, the generator, and the two sets of water wheel structures, as shown in Fig. 3. In addition, the initial design concept in this study was data consideration. The researchers assessed the geometry of the market-available DC 12V Model GOSO F50-12V compact generator from Shenzhen Global Technology, and considered the model of the Pico Hydro Generator [13].

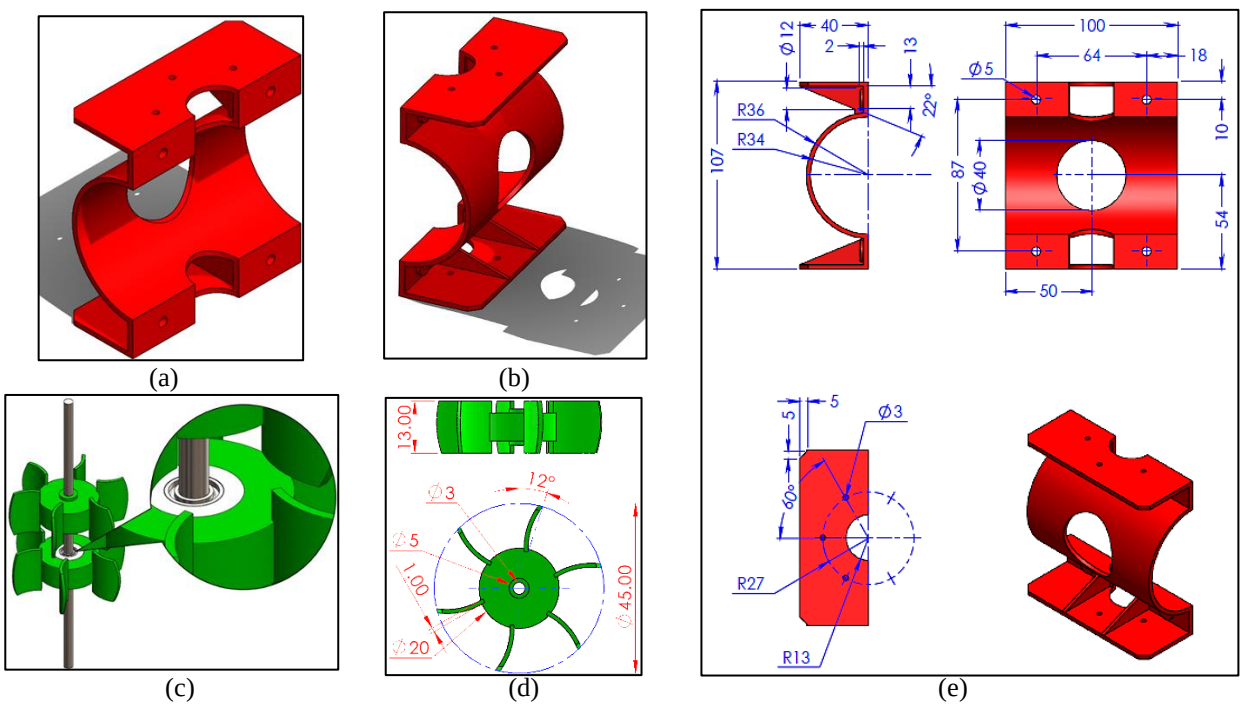

Fig. 3. The vertical-axis water turbine water for installation in pipelines; (a) Left frame, (b) Right frame, (c) Water turbine wheel, (d) Drawing of the water turbine wheel, and (e) Drawing of the left and right frame.

As shown in Fig. 3(c) and 3(d), the researchers studied the design of water turbine wheels based on research on the design and analysis of results for small water turbines producing two horizontal axis wheels using computational fluid dynamics techniques. The research describes the preparation of preliminary models for fluid dynamics analysis, and the method of calculating the angle of placement of water turbine blades [14].

2.3 Research Methods

Before performing rotational analysis, the researchers calculated the angle of impact suitable for use in the design of the propeller placement. According to various propeller profiles such as airfoils 63-212, 4415, Clark Y, and a redesigned wheel blade, the KMUTT Blade was selected to create domain C, and the bias type properties were assigned to the area of domain C for the mech formation of the flow field. The result was obtained, as shown in Fig. 4.

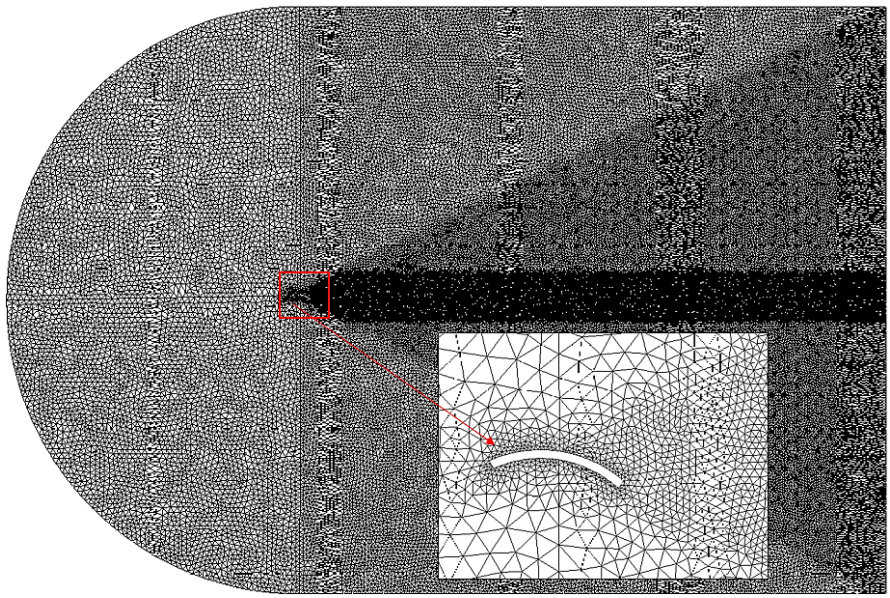

Fig. 4. The mash element for domain C.

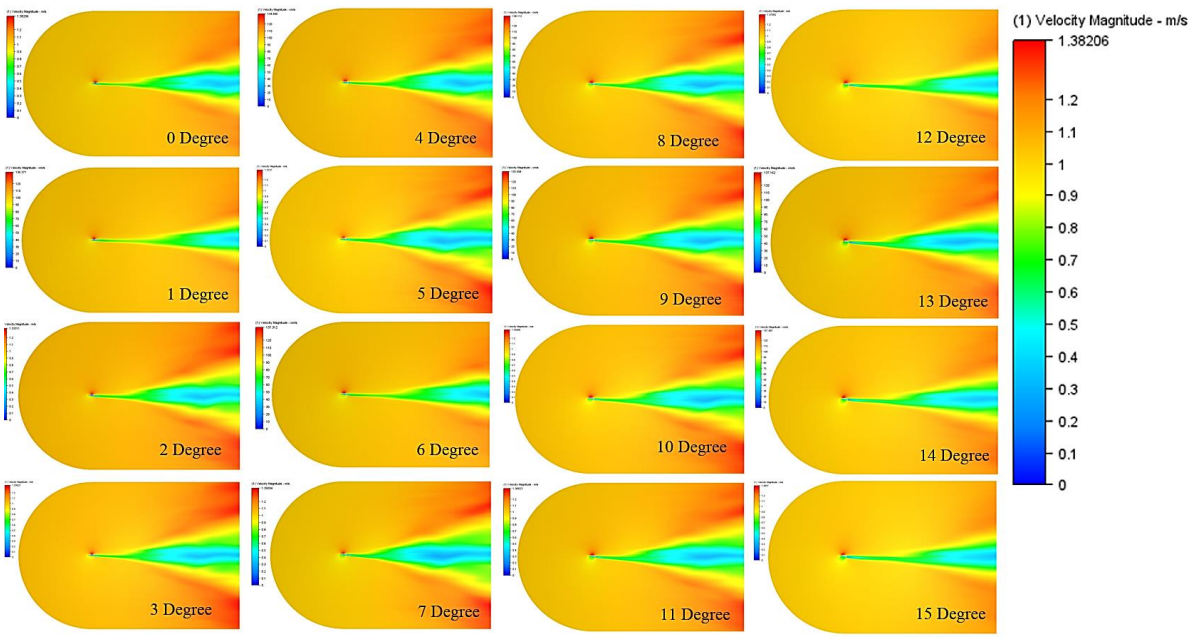

Fig. 5. The velocity contour results of the flow field within the domain C [15].

From Fig. 5. The static pressure of the water is simply the weight per unit area under consideration. In this work, the amalgamation of static and dynamic pressure is known as total pressure. In the simulation, the researcher determines the angle from 0 to 15 degrees to be used for analysis to determine lift force and drag force. In this section, we will consider the angle starting at 0 degrees. So, at an angle of attack of zero degrees, we obtain that the contours of static pressure over an air-foil and KMUTT blade are symmetrical for the upper and lower sections, and the stagnation point is exactly at the nose of the air-foil and the KMUTT blade. Hence, there is no pressure difference created between the two faces of the air-foil and the KMUTT blade at zero degrees of an angle of attack.

Regarding the analysis of the C-domain model, for the flow field on various blade shapes, the KMUTT blade redesigned wheel blades were able to produce the highest L/D ratio at an angle of 12 degrees. Figure 6 presents the analysis results, and Fig. 7 shows the design of the blade placement position. The model blade and a wheel with a diameter of 44 millimetres were assembled.

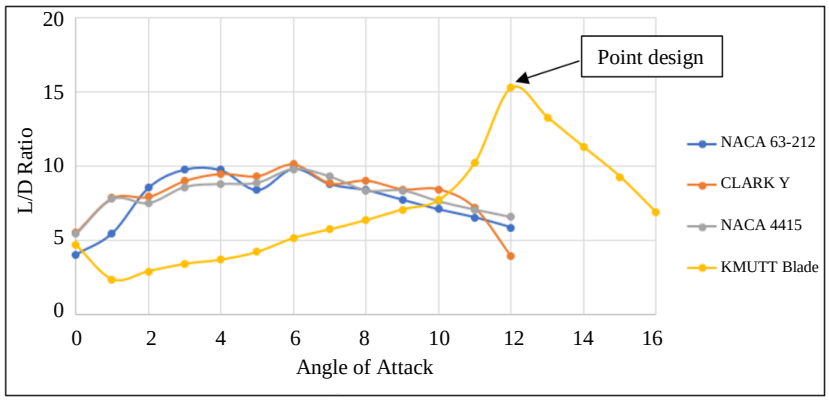

Fig. 6. Analysis results for optimal battering angles [15].

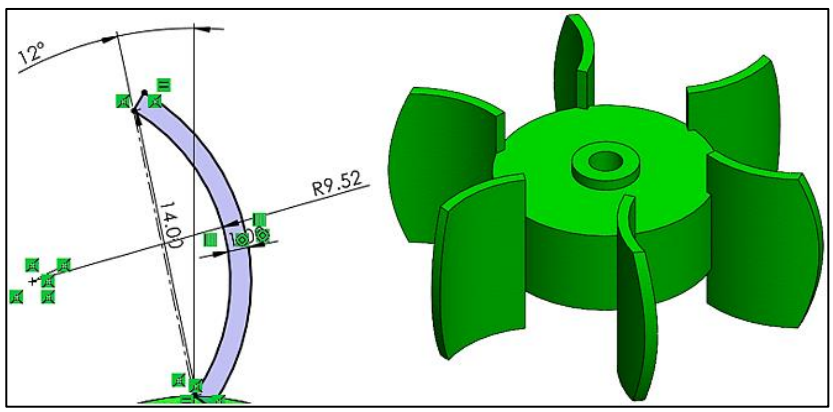

Fig. 7. The result of a small water turbine wheel design.

After obtaining the desired analytical model, the next step is to analyze the rotation of the water domain and the water wheel turbines installed in the piping system. The analysis of the water domain and the set of the water wheels in this study was found to be layered. Therefore, the SST $k-\omega$ turbulence model [16] was used to test and compare the results with the standard $k-\varepsilon$ model. The research process is as follows:

2.3.1 Boundary Condition

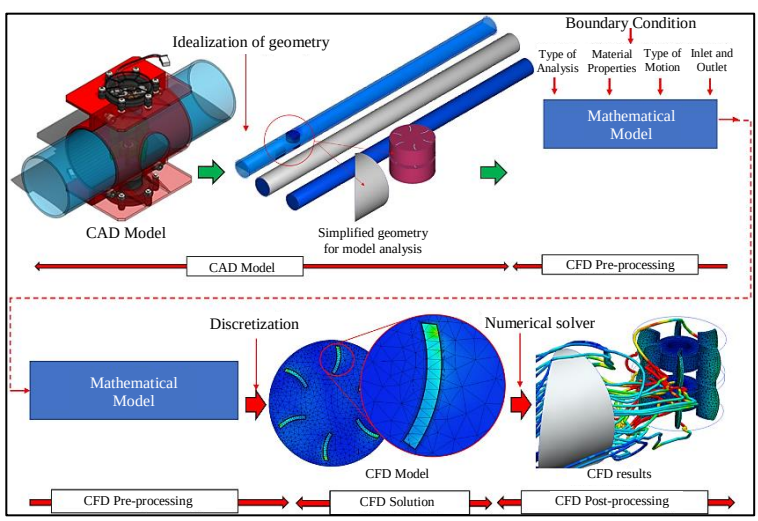

(a)

Fig. 8. Numerical simulation setup; (a) Schematic diagram of the analysis of computational fluid dynamics, (b) Boundary condition, and (c) Angle of attack on the deflector domain.

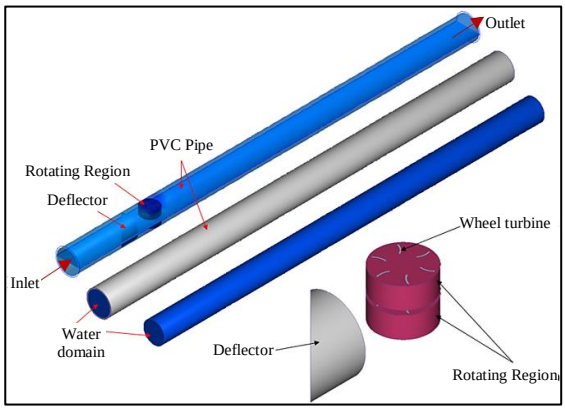

(b)

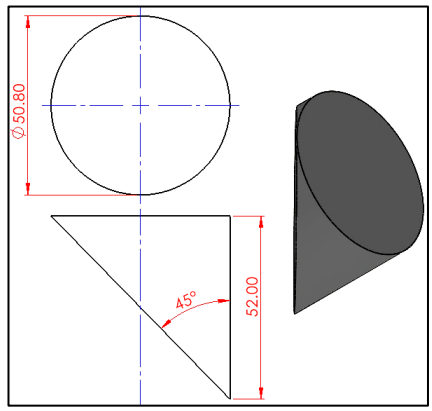

(c)

Fig. 8. (continued) Numerical simulation setup; (a) Schematic diagram of the analysis of computational fluid dynamics, (b) Boundary condition, and (c) Angle of attack on the deflector domain.

Figure 8(a) depicts a schematic diagram of the computational fluid dynamics analysis. The researchers determined and reshaped the domains of the analytic models, and their idealization of geometry makes it easy to calculate by focusing on adjusting the shape of the parts: the tubular domain, the water domain, the deflection domain, the domains of the two rotating regions, and the domain of the water wheel. In the next step, the researchers determined the material properties, the rotation relationship, boundary conditions, and the creation of a mesh for different analysis domains as follows:

PVC pipe domains have solid properties, a density of 1,400 kg/m3, a specific heat of 1,250 J/kg-K, and an emissivity coefficient of 0.92. The water domain has the property of being an incompressible fluid. The incompressible fluid has a density of 999.875 kg/m3, a viscosity of 0.001003 Pa-s, a conductivity of 0.6 W/m-k, specific heat of 4,182 J/kg-K, and an emissivity coefficient of 1.

Deflector domains and water turbine wheels are made of ABS plastic material with solid properties and a density of 1,050 kg/m3, specific heat of 2,050 J/kg-K, and emissivity coefficient of 0.469. The deflector domain opening at d = 50.8 mm is at a 50° angle. The boundary conditions are presented in Fig. 8(b), for the inlet and the volume flow rates are 0.00134, 0.0015, 0.00167, 0.00184, and 0.002 m3/s, respectively. The conditions for the outlet, defined as pressure, are equal to 0 Pa. The rotation conditions of the two rotating regions are defined to rotate in the Y-axis direction, and the scenario type is set up to find rotational speed, defined as a rotation speed based on calculations obtained from volume flow rates. These are 291.88, 326.75, 363.05, 401.27, and 435.67 RPM, respectively. The rotational speed of the water turbine wheel set can be calculated from Equation 1 below [16-18]:

$$N = \frac{\omega \times 60}{2\pi} \tag{1}$$

were; N, is the rotation speed (rpm), $\omega = V/R$, is the angular velocity (rad/s), V, is the velocity (m/s), and R, is the wheel radius of the water turbine (m).

An example of calculating the rotational speed of a water turbine wheel set can be shown below.

Data: 1. Wheel diameter = 40 mm; R = 0.02m.
2. Pipe diameter 2 inch = 50.8 mm.
3. Water flow rate 0.002 m^3/s.

$$\therefore Q = AV;\ A = \frac{\pi d^2}{4};\ \ \therefore A = \frac{3.14 \times 0.0508^2}{4} \approx 0.0022m^2$$

$$0.002m^3/s = \left(0.0022m^2\right) \times V$$

$$\therefore V = \frac{0.002m^3/s}{0.0022m^2} \approx 0.912m/s$$

$$\therefore \omega = \frac{V}{R};\ \frac{0.912m/s}{0.02m} \approx 45.6rad/s$$

$$\therefore N = \frac{\omega \times 60}{2\pi};\ \frac{(45.6)\times 60}{6.28} \approx 435.67rpm$$

To precisely simulate the flow of the water turbine wheels, improved mesh elements are employed in the water turbine wheel boundary layer and the turbine blade layer. The y^+ theory is applied to design an appropriate mesh element system around the boundary layers. The boundary layers are categorized into four components based on theoretical derivations and practical studies, including the viscous sub-layer ($y^+ \leq 5$), buffer layer ($5 < y^+ \leq 30$), log-law region ($30y^+ \leq 500$) and outer layer [19, 20]. The y^+ is defined as:

$$y^+ = \frac{u_\tau y}{v} \tag{2}$$

Where v is the kinematic viscosity, y is the height of the grid to wall, and u_τ is defined as the friction velocity. The friction velocity defined as

$$u_\tau = \sqrt{\frac{\tau_w}{\rho_w}} \tag{3}$$

Where τ_w is denotes the wall shear stress.

In this case, the mesh element formation conditions are different because the blade and the rotation domain of the water turbine are characterized by layered edges. The researchers then determined the initial mesh element generation to auto size and adjusted the mesh element in each domain as follows: The deflection domain is 0.5, and the rotating region domain, which is the rotation domain, is 0.3, with a wall layer of 10 layers, a layer factor of 0.45 and a layer gradation of 1.5 will result in Figs. 9 and 10. The completed three-dimensional computational mesh is shown in Fig. 10. A minimum mesh quality of 0.3 ensures the simulation's correctness [21].

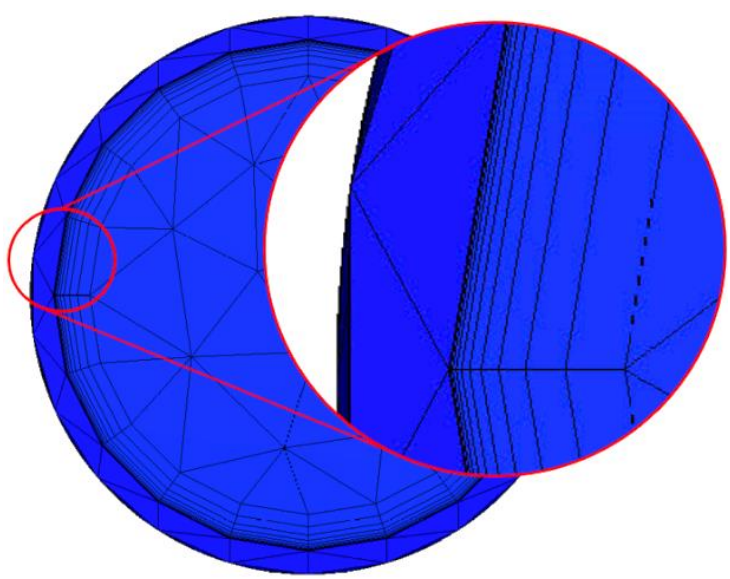

Fig. 9. The mesh element of the PVC pipe.

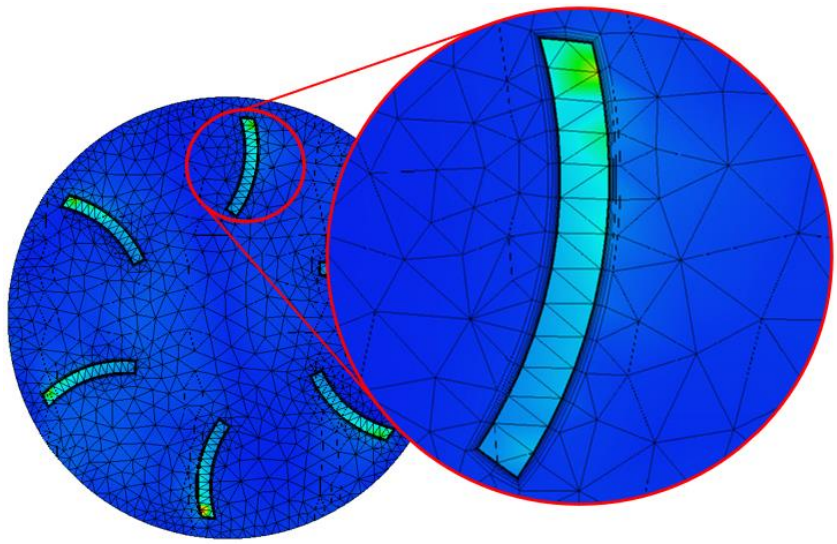

Fig. 10. The mesh element of rotating region.

In this study, the researchers relied on the principle of the rotary mesh element (the moving reference frame). The PVC pipe domain is defined as a stationary domain and designated as stationary wall mesh elements and has no-slip conditions. The method is called the multiple reference frame (MRF). Regarding the determination of calculation schemes, the researchers defined the model as a transient calculation, and the time step is equal to 0.0153 based on the number of propellers, the selection of the standard turbulence model $k-\varepsilon$ and the type turbulence model SST $k-\omega$. The time step for the CFD simulation can be calculaed by using equation (4) below [1, 22, 23].

$$Time\ step = D / (N \times 6) \tag{4}$$

$$\therefore Time\ step = 40/(435.67 \times 6) \approx 0.0153 s$$

3. Theory for Analysis

3.1 Governing Equation for Fluid in the Rotation

The area around the wheelset will have a turbulent flow due to the water fluid, which has incompressible properties. In this approach, the researchers used Reynolds Averaged Navier-Stokes (RANS) equations, which include continuity and momentum equations. To numerically solve these governing equations, simulation tools at present are Ansys Workbench, ANSYS FLUENT, Autodesk Simulation CFD [1, 23], Comsol Multiphysics [1], and SOLIDWORKS Flow Simulation. The basic turbulence model is based on the equation of motion, consisting of the mass equation and the momentum equation [22, 23].

Mass equation.

$$\frac{\partial}{\partial x_i}(\rho u_i) = 0 \tag{5}$$

Momentum equation.

$$\frac{\partial}{\partial x_i}(\rho u_i u_j) = -\frac{\partial P}{\partial x_i} + \frac{\partial}{\partial x_i}\left(\mu\left(\frac{\partial u_i}{\partial x_j} + \frac{\partial u_j}{\partial x_i}\right)\right) + \frac{\partial}{\partial x_i}(-\rho\overline{u_i' u_j'}) \tag{6}$$

where; μ is the Viscosity coefficient, and ρ is the fluid density. Therefore, the momentum equation that is averaged with Reynolds's method is different from the momentum equation that has not yet been averaged, since there is a

diction that arises from the use of the average method of Reynolds, the Reynolds Stresses $\overline{u_i' u_j'}$. It is a definition formed by the value of turbulence in a flow pattern that occurs in various conditions in which the form of the system of equations expresses the Reynolds stress diction, with a form of linear correlation with the value of the rate of change of stress. It can be written as an equation based on Boussinesq's hypothesis [16, 17, 22, 23]:

$$-\rho\overline{u_i' u_j'} = \mu_t\left(\frac{\partial u_i}{\partial x_j}+\frac{\partial u_j}{\partial x_i}\right)-\frac{2}{3}\delta_{ij}\left(\rho k+\mu_t\frac{\partial u_k}{\partial x_k}\right) \tag{7}$$

where; Eddy viscosity value $(\mu)_t$, is the relationship between turbulence kinetic energy values. (k), and the rate of reduction in the kinetic energy value of turbulence (ε). It can be written as follows [16-18, 22, 23].

$$\mu_t = \rho c_\mu \frac{k^2}{\varepsilon} \tag{8}$$

3.2 The Turbulence Model is a $k-\varepsilon$ Model

From the relation of the system, the kinetic energy equation of turbulence. We can write as follows:

$$\frac{\partial}{\partial x_i}(\rho k u_i) = \frac{\partial}{\partial x_i}\left(\left(\mu+\frac{\mu_t}{\sigma_k}\right)\frac{\partial k}{\partial x_i}\right)+G_k+G_b-\rho\varepsilon \tag{9}$$

When the rate decreases in the kinetic energy of the turbulence value, we were able to write the equation as follows:

$$\frac{\partial}{\partial x_i}(\rho\varepsilon u_i) = \frac{\partial}{\partial x_i}\left(\left(\mu+\frac{\mu_t}{\sigma_k}\right)\frac{\partial \varepsilon}{\partial x_i}\right)+\left(C_{\varepsilon 1}\frac{\varepsilon}{k}\left(G_k+C_{\varepsilon 3}G_b\right)\right)\frac{\varepsilon}{k}-\rho C_{\varepsilon 2}\frac{\varepsilon}{k} \tag{10}$$

where;

$$G_k = -\rho\overline{u_i' u_j'}\left(\frac{\partial u_j}{\partial x_i}\right) \tag{11}$$

$$G_b = -g_i\frac{\mu_t}{\rho\,\mathrm{Pr}_T}\frac{\partial \rho}{\partial x_i} \tag{12}$$

When various constants in a system of equations are given, the constants of Launder and Sharma [12, 22, 23] are as follows: C_μ = 0.09, $C_{\varepsilon 1}$ = 1.44, $C_{\varepsilon 2}$ = 1.92, $C_{\varepsilon 3}$ = 1, σ_k = 1, σ_ε = 1.3, σ_T = 0.9.

3.3 The Turbulence Model is a SST k-ω Model (SST, Shear Stress Transport Turbulence Model)

From Menter's turbulence model [20, 22, 23], so is the kinetic energy equation of turbulence (k). It can be written as follows:

$$\frac{\partial}{\partial x_i}(\rho k u_i) = \frac{\partial}{\partial x_i}\left(\left(\mu+\sigma_k\mu_t\right)\frac{\partial k}{\partial x_i}\right)-\rho\overline{u_i' u_j'}\frac{\partial u_j}{\partial x_i}-\rho\beta^* k\omega \tag{13}$$

Equation of the reduction rate of kinetic energy of specific turbulence (ω). It can be written as follows:

$$\frac{\partial}{\partial x_i}(\rho\omega u_i) = \frac{\partial}{\partial x_i}\left(\left(\mu+\sigma_\omega\mu_t\right)\frac{\partial \omega}{\partial x_i}\right)-\frac{\alpha}{\nu_t}\rho\overline{u_i' u_j'}\frac{\partial u_j}{\partial x_i}-\rho\beta\omega^2+2\left(1-F_1\right)\rho\sigma_{\omega,2}\frac{1}{\omega}\frac{\partial k}{\partial x_j}\frac{\partial \omega}{\partial x_j} \tag{14}$$

where the Eddy viscosity variable value is written as [20, 22, 23].

$$\mu_t = \rho \frac{k}{\omega} \frac{1}{\max\left[\frac{1}{\alpha^*}, \frac{\Omega F_2}{a1\omega}\right]} \tag{15}$$

where;

$$\Omega = \sqrt{\Omega_{ij}\Omega_{ij}} \tag{16}$$

$$\Omega_{ij} = \frac{1}{2}\left(\frac{\partial u_i}{\partial x_j} - \frac{\partial u_j}{\partial x_i}\right) \tag{17}$$

$$F_2 = \tanh\left(\Phi_2^2\right) \tag{18}$$

$$\Phi_2 = \max\left[2\frac{\sqrt{k}}{0.09\omega y}, \frac{500\mu}{\rho\omega y^2}\right] \tag{19}$$

From Reynolds's system of stress equations, Boussinesq's hypothetical phenomena can be written [16-18, 20-23], as in equation (3). The constants depicted in the equation system are: $\beta^*, \sigma_k, \sigma_\omega$, and it can be calculated from equation (16), where; θ, the variable value is any constant used in the equation, and the variable value (θ_1) is a constant that comes from the type model SST $k-\omega$. The variable value (θ_2) is a constant derived from the standard turbulence model type $k-\varepsilon$. The variable value (θ) can be obtained from Equation 20.

$$(\theta) = F_1(\theta) + (1 - F_1)(\theta_2) \tag{20}$$

where;

$$F_1 = \tanh\left(\Phi_1^4\right) \tag{21}$$

$$\Phi_1 = \min\left[\max\left(\frac{k}{0.09\omega y}, \frac{500\mu}{\rho y^2 \omega}\right)\left(\frac{4\rho k}{\sigma_{\omega,2} D_\omega^+ y^2}\right)\right] \tag{22}$$

$$D_\omega^+ = \max\left[2\rho\frac{1}{\sigma_{\omega,2^\omega}}\frac{\partial k}{\partial x_j}\frac{\partial \omega}{\partial x_j}, 10^{-20}\right] \tag{23}$$

The other constants in the equation are as follows: $\beta_1 = 0.075$, $\beta_2 = 0.0826$, $a_1 = 0.31$, $a^*=1$.

Table 1 shows the calculation of the torque output obtained from a vertical-axis small water turbine by using the CFD technique, and Table 2 illustrates the mechanical power of a vertical-axis small water turbine installed in a pipeline, which can be calculated from Equation 24.

$$P = \eta \times \Delta p \times Q \tag{24}$$

where; P, is the mechanical power (watt), η, is the mechanical efficiency (%), ΔP, is the pressure drop (Pa), and Q, is the volume flow rate (m^3/s) [15, 24].

4. Results and Discussion

4.1 The Mesh Element Test on the Accuracy

In Fig. 11, the graph shows the relationship between the number of mesh element, the rotation speed and the power output of the vertical-axis small water turbine over a range of 100,000 to 900,000 element. As can be observed, the slope becomes constant when the number of model elements reaches 700,000. So, 900,000 elements were used in the CFD simulation [24].

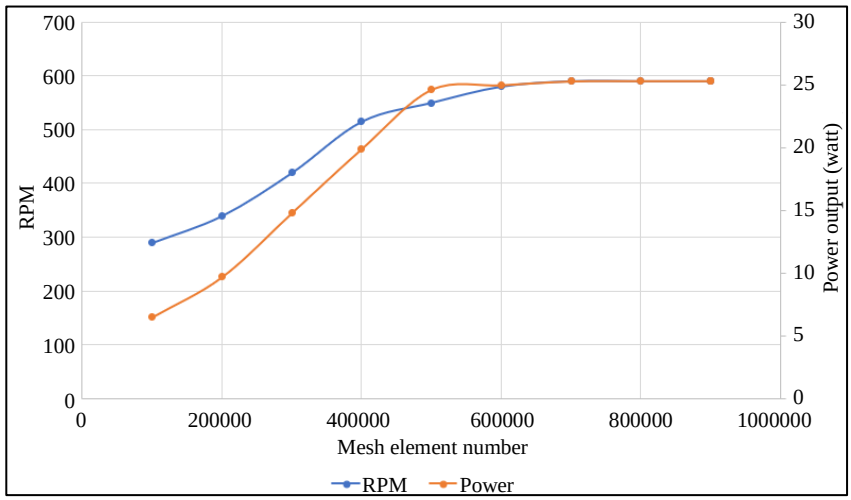

Fig. 11. The graph of mesh elements test results at Q = 0.002 m^3/s [24].

Figure 11 displays that an increase in the number of mesh elements would affect the appropriate and accurate results for analyzing water turbines in this study. From the graph of the power output variable derived from numerical simulations in Fig. 11, the researchers have not calculated the loss rate of the water turbine system.

4.2 Torque Calculation, Mechanical Power, and Performance

In the research section, the researchers selected a turbulence model. The two models, the Standard Turbulence Model $k-\varepsilon$ and the Turbulence Type Model SST $k-\omega$, were employed to study the flow field and the results for comparison. As a result of the torque calculation on both wheels, the top wheel (Rotor T) and the bottom wheel (Rotor B), it was found that the first phase of the two models has similar values on both wheels. It is found in the flow rate range of 0.00134 to 0.00150 m3/s but has initial values different in the flow rate range of 0.184 to the flow rate range of 0.002 m3/s. When considering the torque analysis of the two reels, both in the model $k-\varepsilon$ and SST $k-\omega$ sections, it was found that the top wheel produces a higher torque ratio than the lower wheel. The simulation results are shown in Fig 12.

Mechanical power and performance analysis: The results of the calculations showed mechanical power values and performance values. In the early stages of the model, the two wheels have similar values on both wheels. It is found in the flow rate range of 0.00134 to 0.00150 m^3/s but with different starting values in the flow rate range of 0.184 to 0.002 m^3/s, when analyzing the mechanical power and performance values of the two wheels, both in the model $k-\varepsilon$ and SST $k-\omega$ sections. The upper wheel (rotor T) was discovered to produce more mechanical power and better performance than the lower wheel (rotor B), as shown in the simulation results in Figs. 13 and 14.

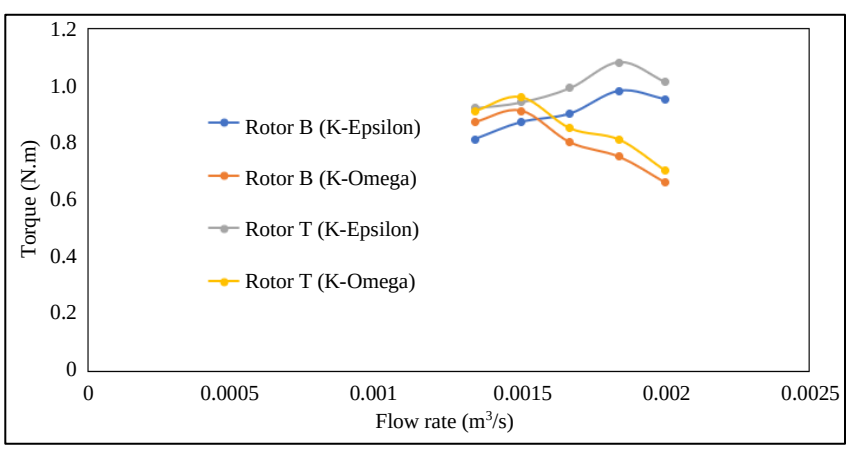

Fig. 12. The calculated torque at different flow rates.

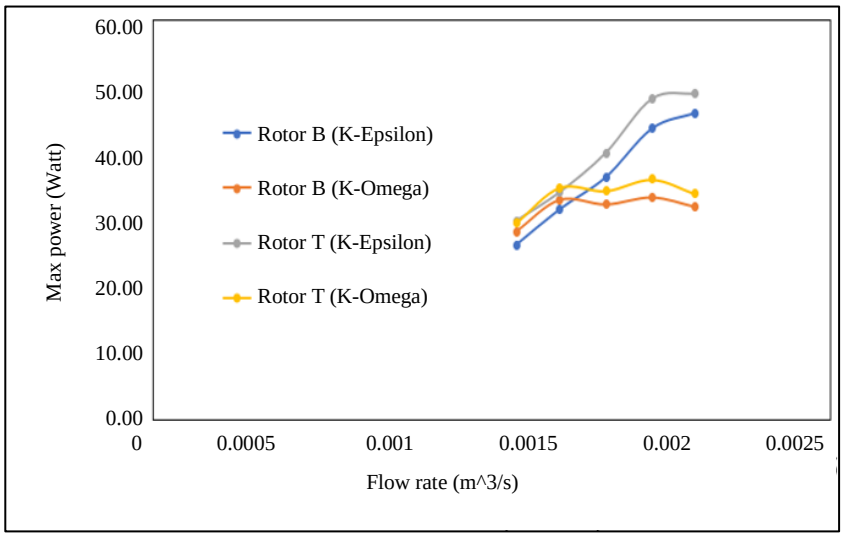

Fig. 13. The calculated mechanical power at different flow rates.

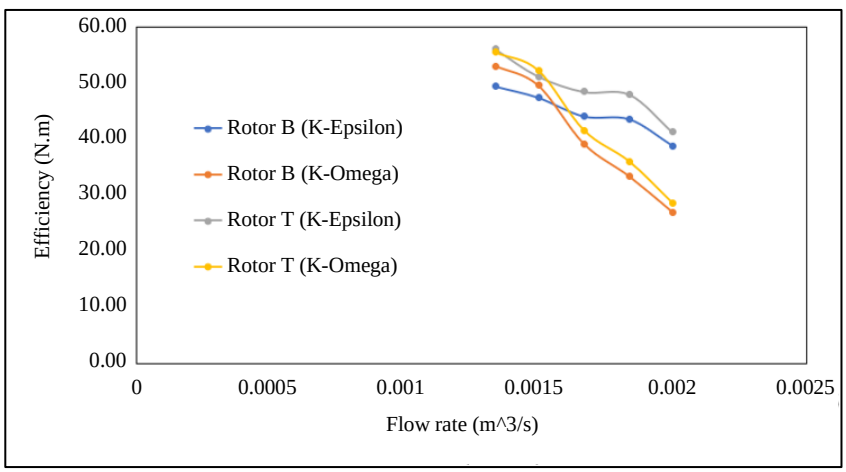

Fig. 14. The calculated performance at different flow rates.

When determining the maximum variables of torque calculation, from Figs. 12-14, the mechanical power and performance were compared to the flow rates of both models, and the results can be summarized in Tables 1-3.

Table 1: The results of the calculations determine the maximum torque values of the turbulence model type ($k-\varepsilon$) and (SST $k-\omega$).

	Flow rate (Q) (m^3/s)	**The maximum torque of the top side wheel**	**The maximum torque of the bottom side wheel**
Turbulence model ($k-\varepsilon$)	0.002	1.08 N.m	0.98 N.m
Turbulence model (SST $k-\omega$)	0.002	0.74 N.m	0.71 N.m

Table 2: The results of the calculations determine the mechanical power values of the turbulence model type ($k-\varepsilon$) and (SST $k-\omega$).

	Flow rate (Q) (m^3/s)	**The maximum mechanical power of the top side wheel**	**The maximum mechanical power of the bottom side wheel**
Turbulence model $k-\varepsilon$	0.002	49.25 watt	44.70 watt
Turbulence model $SST\ k-\omega$	0.002	33.75 watt	32.38 watt

Table 3: The results of the calculations determine the performance values of the turbulence model type ($k-\varepsilon$) and (SST $k-\omega$).

	Flow rate (Q) (m^3/s)	The maximum performance of the top side wheel	The maximum performance of the bottom side wheel
Turbulence model $k-\varepsilon$	0.002	43.58%	48.02%
Turbulence model *SST* $k-\omega$	0.002	49.64%	52.36%

The CAD model for analysis of a novel vertical-axis small water turbine for installation in a pipeline is represented in Fig. 8, while Table 1 summarizes the maximum torque of the two-wheel turbines for both types of turbulence models. Table 2 gives the computed power output. Table 3 shows the mechanical efficiency for the distributions based on time series distributions by using the CFD simulation, where it is determined that the magnitude of the volumetric flow rate influences the turbine rotational speed or angular velocity, as the case may be. The results shown in Tables 1-3 are the results obtained from computational fluid dynamics (CFD) results, indicating the efficiency of the water turbine, and such results have not accounted for the overall operating system loss rate.

4.3 CFD Results

The section presents the results of the simulation of the flow field of the turbulence model $k-\varepsilon$ and SST $k-\omega$. For the rotational velocity analysis and the pressure fields of novel vertical-axial small water turbines for power generation, the two-inch pipe used for the numerical analysis was one meter long, the two water turbine wheels, in this case, are 44 millimeters in diameter, and the total number of mesh elements for analysis is 0.5 million thousand elements. The numerical results are shown in Figs.15-24.

4.3.1 Plot Contour of the Model Rotation Velocity Field $k-\varepsilon$ and SST $k-\omega$.

Fig. 15. Comparison of rotational velocity fields at flow rates of 0.00134 m^3/s.

Fig. 16. Comparison of rotational velocity fields at flow rates of 0.00150 m^3/s.

Fig. 17. Comparison of rotational velocity fields at flow rates of 0.00167 m^3/s.

Fig. 18. Comparison of rotational velocity fields at flow rates of 0.00184 m^3/s.

Fig. 19. Comparison of rotational velocity fields at flow rates of 0.00200 m^3/s.

4.3.2 Pressure contour of the model $k-\varepsilon$ $^{k-\varepsilon}$ and SST $k-\omega$.

Fig. 20. Comparison of pressure fields at flow rates of 0.00134 m^3/s

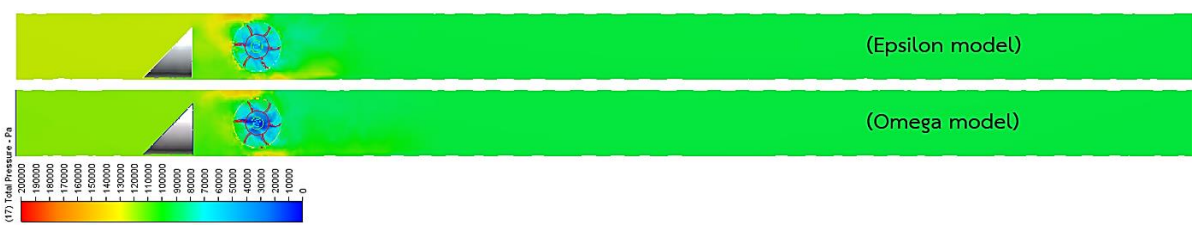

Fig. 21. Comparison of pressure fields at flow rates of 0.00150 m^3/s

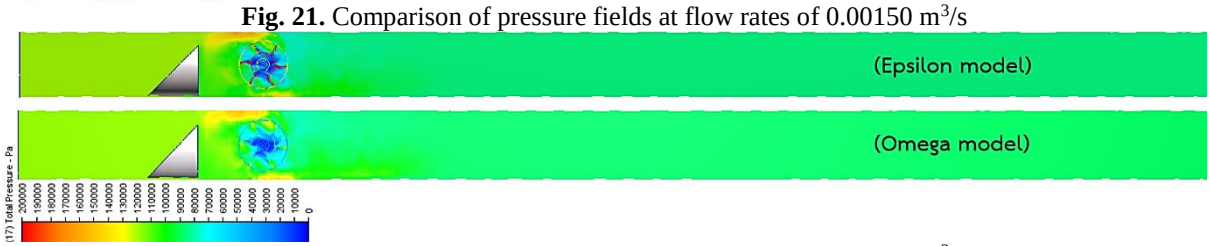

Fig. 22. Comparison of pressure fields at flow rates of 0.00167 m^3/s

Fig. 23. Comparison of pressure fields at flow rates of 0.00184 m^3/s

Fig. 24. Comparison of pressure fields at flow rates of 0.002 m^3/s

Based on the numerical simulation results shown in Fig. 19, the researchers looked at the highest flow rate in the research to be used as data to compare the results of the models $k-\varepsilon$ and SST $k-\omega$ in respect of the average speed at each angle of rotation of the two water wheels. Figure 24 shows the average pressure flow field obtained at different flow rates. Figure 25 illustrates that the turbine wheelset was analysed with an SST turbulence model. The velocity data are obtained at an angle of 0–360 degrees. After that, the researchers then constructed a pressure graph along the length of the tube, according to the results of a numerical simulation of the fluid dynamics of the average pressure flow field obtained from Fig. 24, starting at the entrance and ending at the exit area, as shown in Fig. 26.

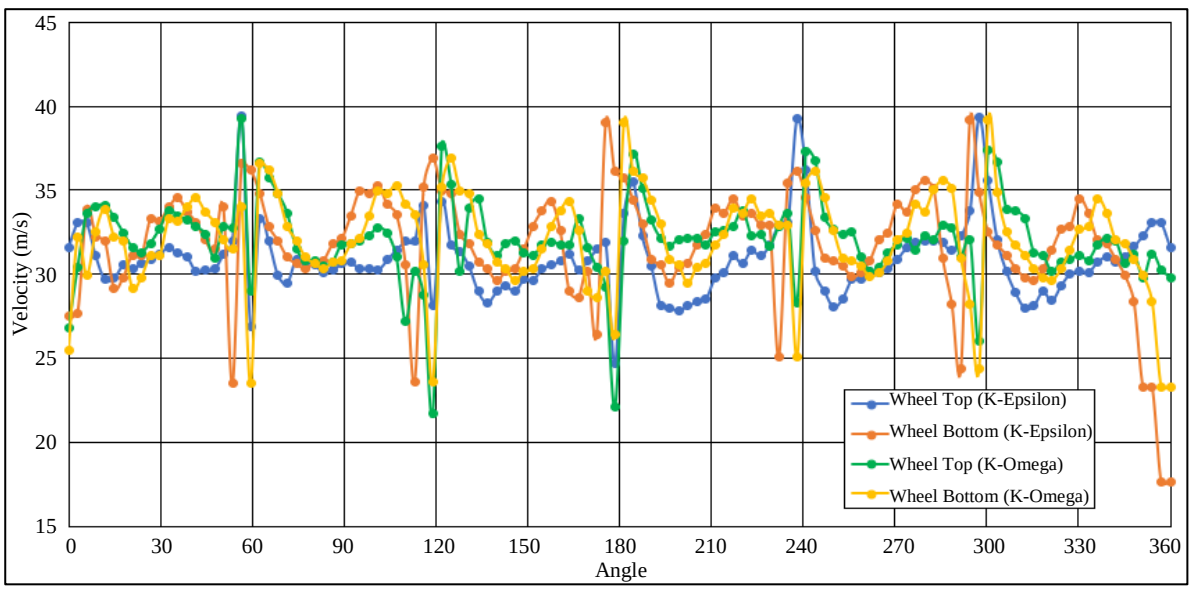

Fig. 25. Compare the speed in each degree of rotation speeds of the model $k-\varepsilon$ and SST $k-\omega$ at a flow rate of 0.002 m^3/s

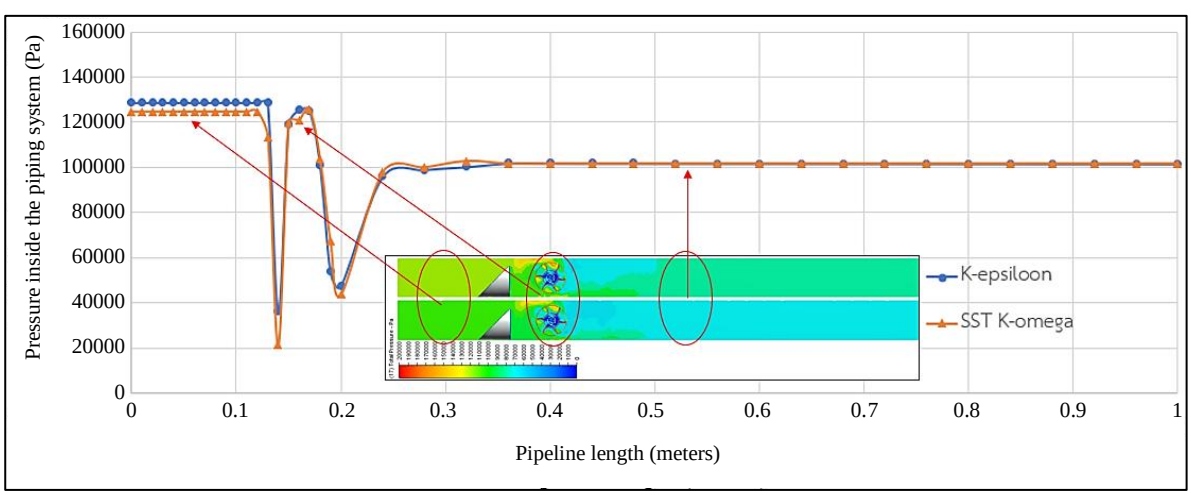

Fig. 26. Compare the pressure fields according to the tube length of the model $k-\varepsilon$ and SST $k-\omega$ at a flow rate of 0.002 m^3/s

The results of the pressure field inside the pipeline where the turbine was installed were obtained from this research and were used to compare with the research of Oladosu and Koya [1]. He conducted a study on the simulation of lift-based spherical turbines installed in 100- and 250-mm pipelines with the SST k-omega model. The result showed that the pressure flow field in the area behind the rotation of the water turbine wheels unit had a similar significantly reduced value.

In this research, when we consider the rate of loss within the pipe system, pipe fittings such as aerator wheels, power shafts, and deflectors can therefore be calculated for the mechanical power as shown in the calculation example below. The example calculation below shows an example of the actual power generation of a vertical-axis small water turbine generator installation in pipeline systems. Furthermore, the authors' estimations of the extracted power showed actual real cases. Table 2 shows the power output of the vertical-axis small water turbine for installation in the pipeline. The relationship between the CFD simulation and Equation (24) can be used to calculate the power output.

Data:

1. From Table 3, the researcher uses an average efficiency of the k-omega turbulent model of 51% (0.51) for calculation in this case.
2. Loss of pressure head (h_L)= 0.907 m. In this study, the average pressure of head loss, as well as the major and minor losses, are defined in the pipe systems of the water turbine.
3. Density of fluid (ρ) = 1,000 kg/m^3
4. Water flow rate (Q)= 0.002 m^3/s.

$$\Delta P = \rho g h_L;$$

$$\therefore \Delta P = 1,000 \times 9.81 \times 0.907 \approx 8,898 Pa.$$

$$P = \eta \times \Delta P \times Q;$$

$$\therefore P = 0.51 \times 8,898 \times 0.002 \approx 9.08 Watt$$

From the calculation of the actual mechanical power produced by Equation (24), it was found that the reduced value was because it took into account the rate of loss from the pipe system. When compared with the CFD calculation results in Table 2, the SST $k-\omega$ turbulence model was selected for comparison with the manual-calculated results. The comparison results showed that the difference was 72.78%. If the resolution of the mesh elements in the rotation zone is set to a higher resolution value, when computing numerical results via CFDs, the results are more accurate but require more computational time and resources. Figure 11 illustrates the mesh element used in this study, which is equal to 900000.

Figure 25 showed that the turbine wheelset was analyzed with a $k-\varepsilon$ and SST $k-\omega$ turbulence model. The velocity data are obtained at an angle of 0-360 degrees. The results showed that the bottom side wheelset had a minimum average speed compared to the top side wheelset in the same model. Since the top side wheelset can generate good rotation speeds and has fluid separation conditions around the propeller and the wheel that rotates less, it does not cause air outlets that result in a loss of efficiency in the work operating system. When comparing the results of the turbulence model $k-\varepsilon$ of the two wheels with the turbulence model SST $k-\omega$, it was found that the upper turbine wheel modeled with $k-\varepsilon$ had a range of velocities. But the degree of rotation was close to that of the turbulence model SST $k-\omega$, for this reason, it can be explained that the turbulence model $k-\varepsilon$ is a starting model that is used to simulate flows with mean characteristics and also uses a small recalculation interval. In the turbulence model $k-\varepsilon$, there are also some drawbacks. Specifically, when considering the hypothesis of Boussinesq, pressure-strain, isotropic, and wall functions, it was found that when the model is analyzed with a 3D specimen with a strongly isolated rotational flow, the result is not very accurate. It is wise to opt for models with a higher order. Figure 26 is a simulation to compare pressure fields along the tube length of the turbulence model $k-\varepsilon$ and SST $k-\omega$, considering a maximum flow rate of 0.002 m^3/s, was found to have similar values. The results from the numerical simulations obtained in Fig. 19 can be used to create a 3D isometric display pattern to simulate particle traces, and the result is given in Fig. 27.

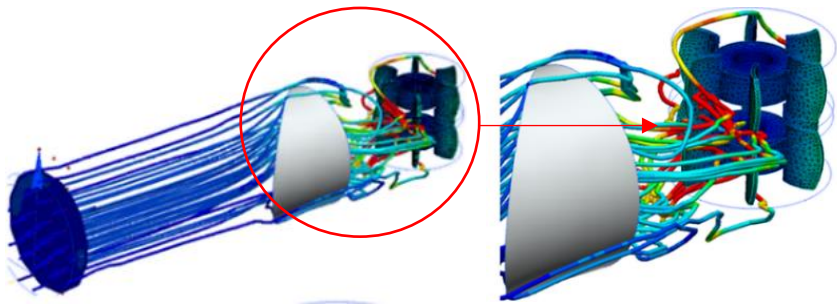

Fig. 27. The particle traces results.

Examples of applications for using the vertical-axis small water turbines for installation in pipeline can be seen in Fig. 28. Figure 28(a) shows a vertical core water turbine mounted to a PVC pipe system in the vertical axis direction, while Fig. 28(b) shows a vertical core water turbine mounted to a PVC pipe system in the horizontal axis direction.

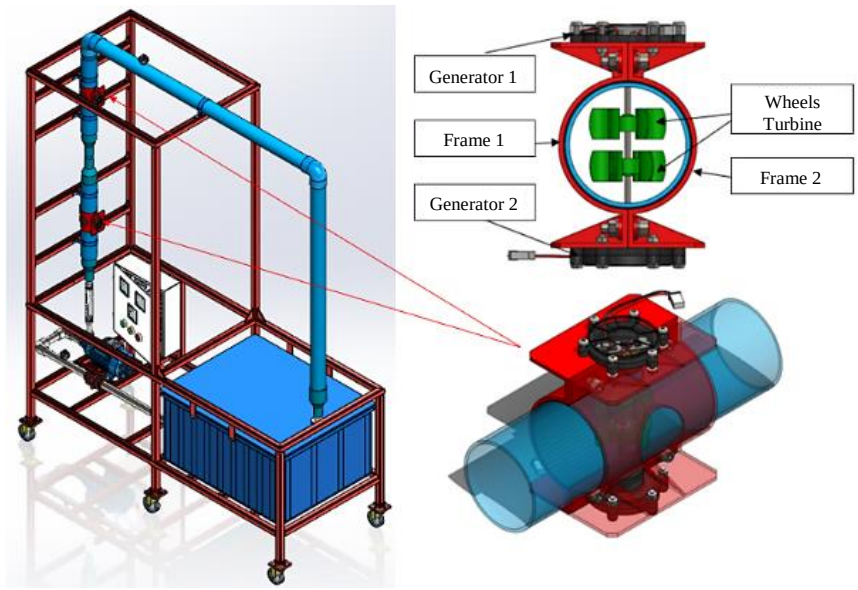

(a) Water turbine installation model for the vertical-axial pipelines.

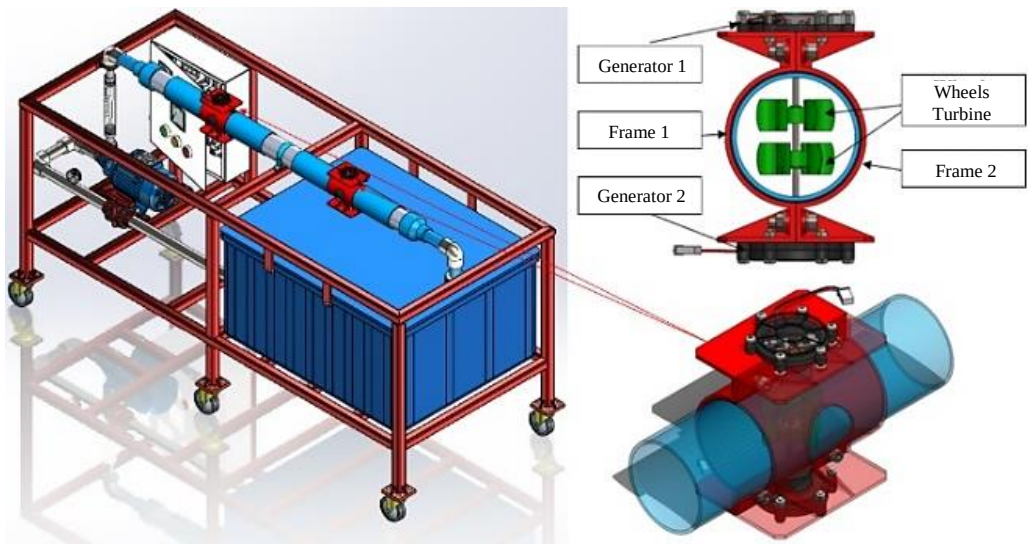

(b) Water turbine installation model for horizontal axial pipelines.

Fig. 28. Applications for a vertical-axis small water turbines to be installed in the water pipeline [24].

5. Conclusion

The data consideration concept for the design was the priority of this study. The researchers assessed the geometry of the market-available DC 12V Model GOSO F50-12V tiny generator obtained from Shenzhen Global Technology. In part 2, the researchers analyzed the data while keeping the installation site in mind, so that it could be appropriately incorporated into the pipeline. Optimal design results led to accurate numerical analysis. Based on the results of numerical simulations of computational fluid dynamics of the vertical-axial water turbines for generating electricity from the water pipelines of both turbulence models, the turbulence model $k-\varepsilon$ was discovered to take longer to calculate the results than the SST $k-\omega$ -type turbulence model. As a result of the simulation results, the calculation variables had an error in some cases, while the turbulence model (SST $k-\omega$) took more time to calculate the results. Because this model tends to have the ability to simulate the near-surface effects of layered walls, the requirements of this research stipulate that the walls of the propeller and the rotation domain are defined as the layered edges of the rotational mesh flow, as shown in Figs. 9 and 10, for example. When analyzing the results according to the replication method, the Multiple Reference Frame (MRF) could simulate the flow of the rotational velocity field. Besides, the pressure was better than the standard turbulence model $k-\varepsilon$. However, the results of computational fluid dynamics were derived from the standard turbulence model $k-\varepsilon$ and SST $k-\omega$, which are merely hypotheses made through simulation with mathematical models. Therefore, for more accurate test results it is recommended that actual testing should be calibrated in the future.

Nomenclature

y	height of the grid to wall, (mm)
y^+	y-plus,
u_T	friction velocity, (m/s)
ω	angular velocity, (rad)
ΔP	pressure drop, (Pa)
τ_w	wall shear stress,
h_L	loss of pressure head, (m)
η	efficiency, ($\%$)
Q	volume flow rate, (m^3/s)
N	rotation speed (RPM)
A	pipe cross-sectional area, (m^2)
V	water speed, (m/s)
R	radius of the water turbine wheel, (m)
D	diameter of the water turbine wheel, (m)
v	Kinematic viscosity ($Pa.s$)
P	power output, ($Watt$)

Acknowledgment

The researchers would like to thank all who assisted in this study, including the team at the Division of Energy Technology, School of Energy, Environment, and Materials, King Mongkut's University of Technology Thonburi, who supported the work and helped obtain a high-quality and accurate analysis. Additionally, the authors would like to thank all the friends who gave support and motivation. The first author would also like to thank his family for their spiritual encouragement throughout the process of writing this paper.

References

[1] Oladosu TL, Koya OA. Numerical analysis of lift-based in-pipe for predicting hydropower harnessing potential in selected water distribution networks for waterlines optimization. Eng Sci Technol Int J. 2018;21(4):672-678.

[2] Muhammad SA, Muhammad AK, Harun J, Faisal J, Alexander C, Kim DH. Design and analysis of in-pipe hydro-turbine for an optimized nearly zero energy building. Sensors. 2021;21(23):8154.

[3] Honggu Y, Woochan S, Soyong S, Young CH, Byung CJ, Cheol-Soo M, et al. Computational analysis of the performance of a vertical axis turbine in a water pipe. Energies. 2019;12(20):3998.

[4] Khan MJ, Bhuyan G, Iqbal MT, Quaicoe JE. Hydrokinetic energy conversion systems and assessment of horizontal and vertical axis turbines for river and tidal applications: a technology status review. Appl Energy. 2009;86(10):1823-1835.
[5] Chen J, Yang HX, Liu CP, Lau CH, Lo M. A novel vertical axis water turbine for power generation from water pipelines, Energy. 2013;54:184-193.
[6] Sammartano V, Arico C, Carravetta A, Fecarotta O, Tucciarelli T. Banki-michell optimal design by computational fluid dynamics testing and hydrodynamic analysis. Energies. 2013;6(5):2362-2385.
[7] Ramos HM, Mello M, De PK. Clean power in water supply systems as a sustainable solution: from planning to practical implementation. Water Supply. 2010;10(1):39-49.
[8] Bahaj AS, Molland AF, Chaplin JR, Batten. Power and thrust measurements of marine current turbines under various hydrodynamic flow conditions in a cavitation tunnel and a towing tank. Renew Energ. 2007;32(3):407-426.
[9] Jawad LH. Performance analysis of in-pipe spherical water turbine used for hydropower generation system. AIP Conf Proc. 2022;2386(1):040042.
[10] EL-Sayed Hussein IIM, Ahmed Farouk AR. In-pipe micro-hydropower systems for energy harvesting. 4th IUGRC International Undergraduate Research Conference; 2019 Jul 29 - Aug 1; Cairo, Egypt. Cairo: Faculty of Engineering, Zagazig University; 2019. p. 1-4.
[11] Lun Cen Z, Gang Zhao J, Xian Shen B. A comparative study of omega RSM and RNG k–epsilon model for the numerical simulation of a hydrocyclone. Iran J Chem Chem Eng. 2014;33(3):53-61.
[12] Sammartano V, Arico C, Carravetta A, Fecarotta O, Tucciarelli T. Banki-michell optimal design by computational fluid dynamics testing and hydrodynamic analysis. Energies. 2013;6(5):2362-2385.
[13] Koya OA, Oladosu TL. Hydropower potentials of water distribution networks in some public universities: a case study. Leonardo Electron J Pract Technol. 2017;30:287-298.
[14] Ramos HM, Mello M, De PK. Clean power in water supply systems as a sustainable solution: from planning to practical implementation. Water Supply. 2010;10(1):39-49.
[15] Lahamornchaiyakul W, Kasayapanand N. Free-Spinning numerical simulation of a novel vertical axis small water turbine generator for installation in a water pipeline. CFD Letter. 2023;15(8):31-49.
[16] Lahamornchaiyakul W. Design and analysis of two-wheel horizontal axis micro water turbine generator using computational fluid dynamics technique. Eng J CMU. 2016;23(1):20-29. (In Thai)
[17] Lahamornchaiyakul W. Application of K-epsilon and K-omega turbulence model for rotation analysis of vertical axis water turbine generator for community. UBU Eng J. 2018;11(1):95-104. (In Thai)
[18] Lahamornchaiyakul W. The CFD-based simulation of a horizontal axis micro water turbine. Walailak J Sci Tech. 2021;18(7):9238.
[19] Yin Z, Esmaeilpour M. The hydrodynamic performance of a turbine in shallow free surface flow. J Hydrodyn. 2021;33(4):804-820.
[20] Menter FR. Two-equation eddy-viscosity turbulence models for engineering applications. AIAA J. 1994;32(8):1598-1605.
[21] Ma T, Yang H, Guo X, Lou C, Shen Z, Chen J, et al. Development of inline hydroelectric generation system from municipal water pipelines. Energy. 2018;144:535-548.
[22] Payambarpour SA, Najafi AF, Magagnato F. Investigation of blade number effect on hydraulic performance of in-pipe hydro savonius turbine. Int J Rotating Mach. 2019;2019:1-14.
[23] Autodesk Inc. Autodesk Simulation CFD, Autodesk Simulation CFD 2015 [Internet]. 2015 [cited 2019 Feb 14]. Available from https://www.autodesk.com/cfd.
[24] Lahamornchaiyakul W, kasayapanand N. The design and analysis of a novel vertical axis small water turbine generator for installation in drainage lines. Int J Renew Energy Deve. 2023;12(2):235-246.